Energy transfer and upconversions in cubic $Cs_2NaYCl_6:Er^{3+}$ and $Cs_2NaErCl_6$

Z. Hasan and L. Biyikli
Department of Physics, Temple University, Philadelphia, Pennsylvania 19122

M. J. Sellars
Laser Physics Center, Research School of Physical Sciences and Engineering, Institute of Advanced Studies, Australian National University, Canberra, Australian Capital Territory 2600, Australia

G. A. Khodaparast
Department of Physics, University of Oklahoma, Norman, Oklahoma 73069

F. S. Richardson and J. R. Quagliano
Department of Chemistry, University of Virginia, Charlottesville, Virginia 22901
(Received 3 December 1996; revised manuscript received 11 April 1997)

Upconversion by two-ion energy transfer, two-photon absorption (TPA), and stepwise absorption processes has been reported for Er^{3+} in cubic Cs_2NaYCl_6 crystal. Blue emission from the $^2G_{9/2}$ and green emission from the $^4S_{3/2}$ state have been observed under the pulsed excitation of $^4F_{9/2}$ in the red. Using a rate equation analysis of the time behavior of the upconverted signal, energy pathways have been determined. On the basis of the time evolution and the concentration dependence of the blue emission a two-ion energy-transfer process has been proposed. TPA in the $^2H_{9/2}$ state ($E>36\,000\ cm^{-1}$) is also observed. However, a resonant one-photon absorption in the $^4S_{3/2}$ state at low temperatures greatly complicates and modifies the TPA spectrum. Fluorescence and excitation spectra associated with $^2H_{9/2}$ and $^4I_{9/2}$ states, and fluorescence lifetimes of various f^n states involved in upconversion processes are also reported. [S0163-1829(97)07232-9]

INTRODUCTION

Energy upconversion processes have been of considerable interest for a long time.[1,2] They have been exploited to produce different colors in phosphors using a single excitation source. Recently, the interest in upconversion materials has been revived because of their applications in producing visible and ultraviolet (UV) lasers while pumping in the infrared (IR) (the upconversion lasers[3,4]). Although in upconversion lasers at least two IR photons are needed to produce one visible or UV photon, the high efficiency of IR laser pumps (diode lasers) under suitable circumstances can more than compensate for low efficiency of upconversion as well as other photon loss mechanisms in a laser cavity. This makes upconversion lasers an attractive alternative to harmonic generation in the visible using nonlinear crystals. Furthermore, with appropriate choice of energy levels and excitation schemes such a process has the potential of producing different UV and vacuum ultraviolet lasers in the high-frequency range while pumping in the visible and IR. An equally important role of the energy transfer in general and the upconversion process in particular is in the depletion of a prepared excited state in an atomic system. Consequently, in all applications where a high excited-state population is necessary, such as multiphoton ionization, laser action, etc., upconversion can be an undesirable process.

For over three decades the focus of upconversion studies has been on triply ionized lanthanide ions in various solid hosts. The unique feature of lanthanide ions is a high density of energy levels in the IR-UV range that allows a variety of upconversion mechanisms to be operative in lanthanide ion doped solids. Among tripositive lanthanide ions, Er^{3+} has one of the richest spectrum in the IR-UV range that makes it ideally suited for energy upconversion studies. IR to visible upconversion in Er has been known for a long time. Successive or stepwise absorption in the IR leads to population buildup in higher levels resulting in red, green, and even blue emissions. Recently, some of these upconversions have been successfully exploited in demonstrating IR pumped red, green, and blue lasers.[3–6]

The list of possible mechanisms for energy upconversion is rather large. We list only a few that are most relevant to the work presented in this paper.

(1) *Stepwise absorption*: For ions in a cubic environment where the lanthanide ions occupy a site of inversion symmetry, electronic transitions within f^n configuration are electric-dipole forbidden. Therefore, at low temperatures excited states have exceedingly long lifetimes, tens of milliseconds in some cases. Upon a powerful excitation by a pulsed laser such states may form a population bottleneck and in the presence of an appropriate energy-level ladder the possibility of stepwise absorption from these states is greatly enhanced. Upconversions by this process are well known for Er^{3+} in many crystalline and glassy hosts.[7–9] They are present in our system as well. The stepwise absorption involves a single ion, and therefore, the upconversion efficiency is independent of the lanthanide ion concentration. Furthermore, for this process to occur, a powerful excitation, such as from a pulsed laser, is not necessary. In fact, it will be more dominant under cw pumping conditions where considerably higher steady-state population of the excited level can be reached.

 © 1997 The American Physical Society

(2) *Two-ion energy transfer*: In this process, two excited Er^{3+} ions exchange energy such that one of the ions is further excited to an even higher energy state while the other relaxes to a lower state. This process will exhibit a quadratic dependence on the power of the exciting radiation as well as a strong dependence on the concentration of the active ions. In other words, upconversion by this process will depend on the probability of finding two Ln^{3+} ions close to each other and at the same time in their excited states. The likelihood of this happening is increased for long-lived states. Furthermore, the time behavior of upconversion would follow the dynamics of the excited states involved.

(3) *Two-photon absorption* (TPA): TPA is another mechanism for upconversion. TPA depends quadratically on the strength of the radiation field and under intense pulsed excitation it will be observed when the sum of the energies of two photons is in resonance with a f^n electronic or vibronic transition. Again, like stepwise absorption, TPA is a single-ion process and it is independent of the concentration of the optically active ions.

After a powerful pulsed laser excitation, such as commonly used in upconversion studies, a complex combination of all of the above processes contributes to upconversion. In general, it is difficult to separate different processes or their respective contributions to the upconversion.

In this paper, we report and analyze energy upconversion processes in Cs_2YNaCl_6:Er^{3+} while exciting Er^{3+} electronic levels in the visible. Upconversion in the blue and green region of the spectrum was observed while exciting the $^4F_{9/2}$ state at about 15 000 cm^{-1} in the red. The time development of the upconverted signal was analyzed to identify the energy levels involved and to separate different mechanisms responsible for upconversion. We also report on two-photon absorption in the $^2H_{9/2}$ state ($E>36\,000\ cm^{-1}$). Some high-lying $4f^{11}$ states that were otherwise inaccessible through single-photon absorption/emission spectra, are observable through upconversion and TPA processes.

One-photon absorption and emission spectra of Cs_2NaYCl_6:Er^{3+} have been reported earlier.[10,11] The crystal host has an elpasolite structure where Er^{3+} sits at the center of an octahedron formed by six Cl^- ions located at the apexes. The cubic coordination is maintained at all temperatures and throughout the range of Er concentrations. Purely electronic f^n transitions are magnetic-dipole allowed and appear as sharp but weak lines. The optical spectrum is dominated by strong vibronic bands associated with the odd parity vibrational modes of the $(ErCl)^{3-}$ complex. These vibronic transitions are electric-dipole allowed. A cubic crystal-field analysis with intensity mechanisms invoked by odd-parity vibrations gives an excellent account of the observed energy positions and intensities of spectral lines.

ENERGY-LEVEL CALCULATIONS

For energy transfer studies it is necessary to know the position of all energy levels involved as accurately as possible. Our previous calculations[10] did not include higher-energy states that became observable due to upconversion processes reported here. Also, it did not include second-order crystal-field effects that considerably improve the crystal-field splittings within some free ion multiplets. We therefore give an outline of an improved calculation that was performed to determine the $4f^{11}$ electronic energy-level structure of Er^{3+} in Cs_2NaYCl_6. We used a model Hamiltonian that operated entirely within the $4f^{11}$ configuration,

$$H=H_a+H_{cf}+H_{ccf}, \tag{1}$$

where H_a is defined to incorporate the isotropic parts of H (including the spherically symmetric parts of the $4f$-electron/crystal-field interactions), H_{cf} is defined to represent the nonspherically symmetric components of the one-electron crystal-field interactions, and H_{ccf} incorporates some partial consideration of two-electron correlation-crystal-field (CCF) interactions into the model Hamiltonian:

$$H_a=\mathbf{E}_{\rm ave}+\sum_k \mathbf{F}^k f_k+\alpha L(L+1)+\beta G(\mathbf{G}_2)+\gamma G(\mathbf{R}_7)$$
$$+\sum_i \mathbf{T}^i t_i+\zeta_{s0}A_{s0}+\sum_k \mathbf{P}^k p_k+\sum_j \mathbf{M}^j m_j, \tag{2}$$

where $k=2,4,6$; $i=2,3,4,6,7,8$; $j=0,2,4$; and each of the interaction operators (shown in boldface) and interaction parameters (shown in italicized notation) is written and defined according to standard practice.[12,13] The $[SL]J$ multiplet structure of the $4f^{11}(Er^{3+})$ electronic configuration is determined predominantly by the H_a part of the model Hamiltonian, whereas mixings between different multiplets and splittings within individual multiplet manifolds are determined by the crystal-field interactions represented in H_{cf} and H_{ccf}.

The one-electron crystal-field interaction Hamiltonian (H_{cf}) employed in this study was defined to reflect the O_h symmetry of the Er^{3+} ions in $Cs_2NaErCl_6$, and in its parametrized form it may be written as

$$H_{cf}=\mathbf{B}_0^4\{C_0^{(4)}+(\tfrac{5}{14})^{1/2}[C_4^{(4)}+C_{-4}^{(4)}]\}$$
$$+\mathbf{B}_0^6\{C_0^{(6)}-(\tfrac{7}{2})^{1/2}[C_4^{(6)}+C_{-4}^{(6)}]\}, \tag{3}$$

where the $C_q^{(k)}$ are intraconfigurational spherical-tensor operators of rank k and order q, and $\mathbf{B}_0^6$ and $\mathbf{B}_0^2$ are one-electron crystal-field interaction parameters. It was found that the crystal-field splittings observed within a number of $4f^{11}[SL]J$ multiplets manifolds cannot be satisfactorily accounted for in terms of any standard, one-electron crystal-field interaction model.[14] However, the incorporation of certain two-electron CCF interactions into the models leads to calculated results in good agreement with experimental observation. Following Ref. 11 and including the most significant term in H_{ccf}, we write H_{ccf} as

$$H_{ccf}=\mathbf{G}_{10A0}^4\{g_{10A0}^{(4)}+(\tfrac{5}{14})^{1/2}\{g_{10A4}^{(4)}+g_{10A-4}^{(4)}\}\}, \tag{4}$$

where the $g_{10Aq}^{(k)}$ are two-electron CCF interaction operators (with $k=4$ and $q=0,\ \pm4$), and G_{10A0}^4 is treated as a CCF interaction parameter.

In the energy-level calculations performed in this study, the model Hamiltonian was diagonalized within the complete set of $4f^{11}SLJM_J$ angular momentum states (a total of 364 states), and various subsets of the Hamiltonian parameters

TABLE I. Calculated and observed crystal-field energy levels of Er^{3+} in $Cs_2Na_xEr_{1-x}Cl_6$. n.d.means not deleted.

Level	Multiplet label[a]	Crystal-field level[b]	Energy (cm^{-1}) Obx[c]	Calc.[d]	Δ[e]	Level	Multiplet label[a]	Crystal-field level[b]	Energy (cm^{-1}) Obs.[c]	Calc.[d]	Δ[e]
1	$^4I_{15/2}$	Γ_8	0	−2	2	37		Γ_8	26 367	26 354	13
2		Γ_7	25	22	3	38		Γ_6	26 425	26 409	16
3		Γ_8	57	56	1	39	$^4G_{9/2}$	Γ_6	n.d.	27 219	
4		Γ_6	259	255	4	40		Γ_8	n.d.	27 262	
5		Γ_8	287	288	−1	41		Γ_8	n.d.	27 306	
6	$^4I_{13/2}$	Γ_6	6 492	6 495	−3	42	$^2K_{15/2}$	Γ_8	n.d.	27 363	
7		Γ_8	6 517	6 521	−4	43		Γ_8	n.d.	27 451	
8		Γ_7	6 532	6 535	−3	44		Γ_7	n.d.	27 531	
9		Γ_8	6 682	6 686	−4	45		Γ_8	n.d.	27 728	
10		Γ_7	6 686	6 693	−7	46		Γ_6	n.d.	27 747	
11	$^4I_{11/2}$	Γ_6	10 166	10 160	6	47	$^2G_{7/2}$	Γ_7	n.d.	27 895	
12		Γ_8	10 174	10 167	7	48		Γ_8	n.d.	27 955	
13		Γ_8	10 238	10 228	10	49		Γ_6	n.d.	27 968	
14		Γ_7	10 238	10 232	6	50	$^2P_{3/2}$	Γ_8	n.d.	31 326	
15	$^4I_{9/2}$	Γ_8	12 345	12 346	−1	51	$^2K_{13/2}$	Γ_6	n.d.	32 555	
16		Γ_6	12 410	12 422	−12	52		Γ_8	n.d.	32 606	
17		Γ_8	12 489	12 494	−5	53		Γ_7	n.d.	32 660	
18	$^4F_{9/2}$	Γ_8	15 152	15 178	−26	54	$^2P_{1/2}$	Γ_6	n.d.	32 716	
19		Γ_8	15 246	15 262	−16	55	$^2K_{13/2}$	Γ_7	n.d.	32 901	
20		Γ_6	15 337	15 333	4	56		Γ_8	n.d.	32 936	
21	$^4S_{3/2}$	Γ_8	18 265	18 258	7	57	$^4G_{5/2}$	Γ_8	n.d.	33 034	
22	$^2H(2)_{11/2}$	Γ_8	19 016	19 020	−4	58		Γ_7	n.d.	33 286	
23		Γ_7	19 049	19 049	0	59	$^4G_{7/2}$	Γ_6	n.d.	33 738	
24		Γ_8	19 140	19 151	−11	60		Γ_8	n.d.	33 808	
25		Γ_6	19 174	19 189	−15	61		Γ_7	n.d.	33 942	
26	$^4F_{7/2}$	Γ_6	20 376	20 381	−5	62	$^2D(1)_{5/2}$	Γ_7	n.d.	34 360	
27		Γ_8	20 446	20 446	0	63		Γ_8	n.d.	34 474	
28		Γ_7	20 467	20 456	11	64	$^2H(2)_{9/2}$	Γ_8	36 133[f]	36 156	−23
29	$^4F_{5/2}$	Γ_8	22 056	22 061	−5	65		Γ_6	n.d.	36 207	
30		Γ_7	22 135	22 112	23	66		Γ_8	36 345[f]	36 345	0
31	$^4F_{3/2}$	Γ_8	22 447	22 456	−9	67	$^4D_{5/2}$	Γ_7	n.d.	38 258	
32	$^2G(2)_{9/2}$	Γ_8	24 428	24 420	8	68		Γ_8	n.d.	38 308	
33		Γ_6	24 462	24 471	−9	69	$^4D_{7/2}$	Γ_6	n.d.	38 753	
34		Γ_8	24 519	24 524	−5	70		Γ_8	n.d.	38 802	
35	$^4G_{11/2}$	Γ_8	26 110	26 108	2	71		Γ_7	n.d.	38 945	
37		Γ_7	26 193	26 197	−4						

[a]Identifies the principal SLJ component of the state vectors.
[b]Irreducible representation of the crystal-field level in the O_h double rotation group.
[c]Experimental observed positions of the assigned crystal-field energy levels.
[d]Energies calculated using the Hamiltonian parameters given in the text.
[e]Difference between observed and calculated energies.
[f]Error margins are $\pm 25\ cm^{-1}$.

were treated as variables in fitting the calculated energy levels to those located and assigned from experiment.

Results obtained from our energy-level calculations (with CCF interactions included) are shown in Table I, along with the locations and symmetry assignments of all levels characterized from experiment. The calculated energies correspond to eigenvalues of the parametrized model Hamiltonian derived from our calculated-to-observed data fits. The atomic and crystal-field Hamiltonian parameters used in our final energy-level calculations are listed below (with all values given in cm^{-1} units). Atomic parameters [as defined in Eq. (2)]: $\mathbf{E}_{ave}=35\ 255$; $\mathbf{F}^2=97\ 197$; $\mathbf{F}^4=69\ 303$; $\mathbf{F}^6=47\ 660$; $\alpha=15.95$; $\beta=-591$; $\gamma=2021$; $\mathbf{T}^2=337$; $\mathbf{T}^3=46.2$; $\mathbf{T}^4=11.9$; $\mathbf{T}^6=-360$; $\mathbf{T}^7=219$; $\mathbf{T}^8=427$; $\zeta_{so}=2355$; $\mathbf{P}^2=699$; $\mathbf{P}^4=524$; $\mathbf{P}^6=350$; $\mathbf{M}^0=5.30$; $\mathbf{M}^2=2.97$; $\mathbf{M}^4=2.01$. Crystal-field parameters [as defined in Eqs. (3) and (4)]: $\mathbf{B}_0^4=1459$; $\mathbf{B}_0^6=162$; $\mathbf{G}_{10A0}^4=-896$.

The energy-level calculations performed in the present study yield results that are in much better agreement with

experiment than those reported in previous studies of Er^{3+} in $Cs_2NaErCl_6$.[10,11] This is due in very large part to our augmentation of the crystal-field Hamiltonian with the CCF interactions represented in Eq. (4). The results obtained here, and in the previous work on Er^{3+} in some other crystalline hosts,[12,14] indicate that these CCF interactions play a major role in determining the crystal-field energy-level structures observed with several $4f^{11}[SL]J$ multiplet manifolds of Er^{3+}.

EXPERIMENT

Pure $Cs_2NaErCl_6$, and dilute crystals of Cs_2NaYCl_6:Er^{3+} were grown in vacuum sealed quartz ampoules by the Bridgeman technique. Details of the method of growth have been described elsewhere.[10,15,16] The crystals grown were high-quality single crystals, a few centimeters long and were highly hygroscopic. The crystals were thinly coated with a silicone-based vacuum grease to protect them from traces of water during the experiment. The grease was transparent in the spectral range of interest and showed no detectable emission under laser excitation. The crystals were stored in an evacuated desiccator or sealed in an evacuated ampoule.

The emission and absorption spectra were recorded using 0.75 m Spex monochromator. For cw excitation a dye laser (Spectra Physics 375) with the DCM dye pumped by an Ar-ion laser (Spectra Physics 165) was used. Time-resolved measurements were performed using a pulsed dye laser (Molectron DLII) pumped by a nitrogen laser (Molectron UV-14). Typical pulse widths were 5–10 ns. The energy resolution was $\sim 0.1\ cm^{-1}$ from both cw and pulsed lasers. This resolution was adequate for the experiments reported here. A gated photomultiplier tube in conjunction with a Princeton Applied Research boxcar integrator was employed for detecting the time-resolved signals. In order to avoid the saturation of the signal during the laser pulse, the photomultiplier tube (PMT) was blinded momentarily by applying a negative potential on the first dynode with respect to the photocathode. For low-temperature measurements the sample was cooled by the flow of cold helium gas that circulated around it. The temperature of the sample was controlled by controlling the flow rate of helium and no heater was used to attain temperatures in the 15–300 K range. Other details of the experiment are the same as reported earlier.[17,18]

$^4I_{9/2}$-$^4I_{15/2}$ TRANSITION

Our earlier work[10] reported all electronic and associated vibronic transitions from the ground $^4I_{15/2}$ state up to the $^4G_{11/2}$ state in the near UV. However, no absorption or emission spectra associated with $^4I_{9/2}$ were reported in our previous studies. This was due to the weak oscillator strength of the $^4I_{15/2}$-$^4I_{9/2}$ transition and the poor response of our detector in the (IR) range. A knowledge of crystal-field energies of $^4I_{9/2}$, its radiative lifetime, and the intensity distribution in the spectrum is essential for distinguishing different mechanisms and pathways possible for energy upconversions; therefore, we studied this transition in detail.

In the present study, we used a red enhanced GaAs tube to monitor the $^4I_{9/2}$-$^4I_{15/2}$ transition. The emission spectrum shown in Fig. 1 was recorded by exciting the $^4F_{9/2}$ state that lies above $15\,000\ cm^{-1}$. The spectrum is resolved enough for detailed assignments.

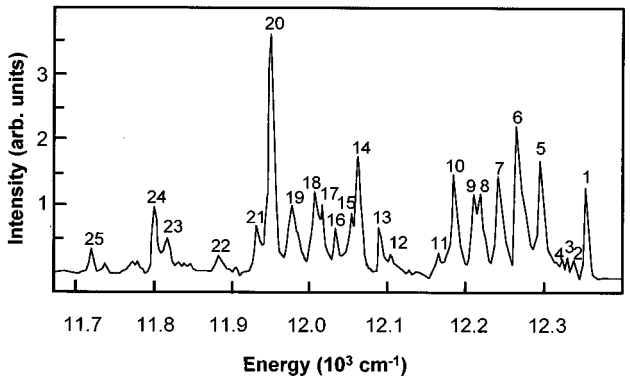

FIG. 1. Emission spectrum for the $^4I_{9/2}$-$^4I_{15/2}$ transition monitored by exciting the $^4F_{9/2}$ state, for Cs_2NaYCl_6:Er^{3+} (12%) at $T = 15$ K. Assignments of different electronic and vibronic peaks are given in Table II.

In $^4I_{9/2}$-$^4I_{15/2}$ emission, Fig. 1, purely electronic f^{11} transitions are sharp but weak as they are only weakly magnetic-dipole allowed; the spectrum is dominated by electric-dipole allowed vibronic transitions arising from three odd-parity vibrational modes of the $(ErCl_6)^{3-}$ complex, $v_3(T_{1u})$, $v_4(T_{1u})$, and $v_6(T_{2u})$, parentheses contain the corresponding irreducible representation of the O_h group. The spectrum in Fig. 1 also shows some vibronic transitions associated with the lattice modes as seen in the spectra associated with the other electronic transitions.[10,11] Furthermore, the interaction of the $(ErCl_6)^{3-}$ vibrational modes with the lattice causes splittings and redistribution of intensities in vibronic lines. Both of these effects complicate vibronic spectra and make the comparisons of the observed and calculated intensities difficult. In our intensity calculations only the $(ErCl_6)^{3-}$ vibrational modes and their coupling to electronic states in a Born-Oppenheimer fashion were considered.[10] It is for this reason that a comparison of the observed $^4I_{9/2}$-$^4I_{15/2}$ spectrum with the simulated spectrum based on our crystal-field and intensity calculations has not been presented here.

Assignments of the $^4I_{9/2}$-$^4I_{15/2}$ emission (Fig. 1) were based on the calculation of crystal-field energy levels described earlier. For vibronic assignments, the separations between the electronic origins and the vibronic lines were compared with the vibrational energies. From our earlier work,[10] energies of the three odd-parity modes are $v_3 = 255\ cm^{-1}$, $v_4 = 110\ cm^{-1}$, and $v_6 = 87\ cm^{-1}$. The assignment of the emission spectrum is given in Table II. The TO-LO splitting of the v_3 mode by $10-15\ cm^{-1}$ is also apparent in the spectrum. Details of the vibronic intensities and conclusions based on them are all consistent with the previously reported results on the absorption and emission spectra of other states in this system.[10,11]

For absorption studies of $^4I_{9/2}$ state a Ti-sapphire laser was used as the excitation source. The absorption spectrum is shown in Fig. 2. It was recorded monitoring the upconverted signals in the blue and green region. As will be described later, these upconversions have quadratic dependence on the intensity of the exciting laser beam. Therefore, relative intensities of different lines shown in Fig. 2 are accord-

TABLE II. Assignments for the $^4I_{9/2}$-$^4I_{15/2}$ fluorescence spectrum of $Cs_2Na_xEr_{1-x}Cl_6$. The asterisk means not assigned, weak.

Transition[a]	Energy (cm^{-1})	ΔE (cm^{-1})[b]	Assignments[c]
1	12 345	0	$^a\Gamma_8 \rightarrow {}^a\Gamma_8$
2	12 335	*	
3	12 325	0	$^a\Gamma_8 \rightarrow {}^a\Gamma_7$
4	12 315	*	
5	12 291	0	$^a\Gamma_8 \rightarrow {}^b\Gamma_8$
6	12 267	82	$^a\Gamma_8 \rightarrow {}^a\Gamma_8 + v_6$
7	12 217	109.8	$^a\Gamma_8 \rightarrow {}^a\Gamma_8 + v_4$
			$^a\Gamma_8 \rightarrow {}^a\Gamma_7 + v_3$
8	12 217	108	$^a\Gamma_8 \rightarrow {}^a\Gamma_7 + v_4$
9	12 210	81	$^a\Gamma_8 \rightarrow {}^b\Gamma_8 + v_6$
10	12 185	106	$^a\Gamma_8 \rightarrow {}^b\Gamma_8 + v_4$
11	12 162	*	
12	12 105	244	$^a\Gamma_8 \rightarrow {}^a\Gamma_8 + v_3$
13	12 090	0.25	$^a\Gamma_8 \rightarrow {}^a\Gamma_6$, or
			$^a\Gamma_8 \rightarrow {}^a\Gamma_8 + v_3$
14	12 061	0.26	$^a\Gamma_8 \rightarrow {}^c\Gamma_8$, or
			$^a\Gamma_8 \rightarrow {}^a\Gamma_7 + v_3$
15	12 052	240	$^a\Gamma_8 \rightarrow {}^b\Gamma_8 + v_3$
16	12 032	259	$^a\Gamma_8 \rightarrow {}^b\Gamma_8 + v_3$
17	12 016	*	
18	12 006	84	$^a\Gamma_8 \rightarrow {}^a\Gamma_6 + v_6$
19	11 978	86	$^a\Gamma_8 \rightarrow {}^c\Gamma_8 + v_6$,
			$^a\Gamma_8 \rightarrow {}^a\Gamma_6 + v_4$
20	11 955	106	$^a\Gamma_8 \rightarrow {}^c\Gamma_8 + v_6$
21	11 933	157	
22	11 891	*	
23	11 817	244	$^a\Gamma_8 \rightarrow {}^b\Gamma_8 + v_3$
24	11 800	261	
25	11 721		

[a]See Fig. 1 for line numbering.
[b]Displacements from zero phonon (origin) lines.
[c]Crystal-field designations are given in Table I.

ingly scaled. Three purely electronic transitions are very sharp and some intense vibronic transitions can also be seen in Fig. 2. This spectrum complimented the emission data and confirmed assignments based on it.

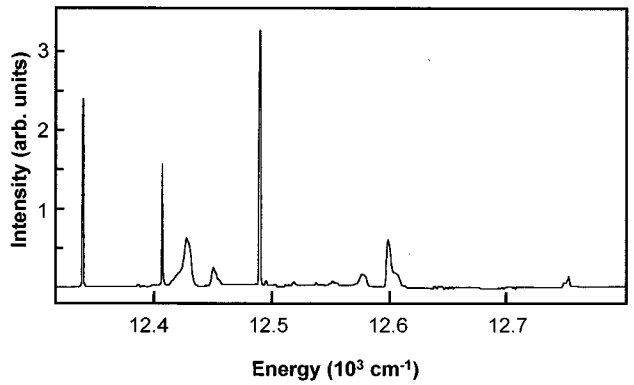

FIG. 2. Excitation spectrum of $^4I_{9/2}$ recording the upconverted signal in the blue and green region, $T = 10$ K.

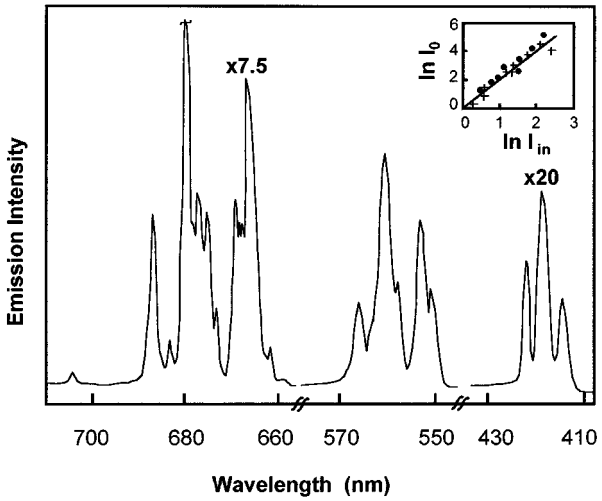

FIG. 3. Low-resolution emission spectrum of the upconverted signal after pulsed excitation of the $^4F_{9/2}$ state. The signal was collected from the excitation region on the crystal to enhance the signal for the blue emission centered at 420 nm. The assignments for the three emission bands are $^4F_{9/2}$-$^4I_{15/2}$ (660–710 nm), $^4S_{3/2}$-$^4I_{15/2}$ (550–570 nm), and $^2G_{9/2}$-$^4I_{15/2}$ (410–430 nm). The inset shows a plot of the upconversion output intensity (I_0) as a function of laser input intensity (I_{in}). Solid circles and crosses represent the blue and the green upconversions, respectively. The solid line shown has a slope of 2 corresponding to the quadratic dependence of the upconversion process on the intensity of the exciting radiation.

UPCONVERSIONS

Energy upconversions were studied by exciting the $^4I_{15/2}$-$^4F_{9/2}$ transition in the red, $\sim 15\,000$–$15\,600$ cm^{-1}, using a pulsed laser. Exciting this transition gave a bluish green appearance to the crystal whenever the laser was in resonance with an electronic or vibronic transition of $^4I_{15/2}$-$^4F_{9/2}$. The effect was an overwhelming change of the color in crystals with high Er concentration, $\geqslant 5$ at. %. Under tight focusing conditions, the crystal had a blue focused spot and a yellowish green appearance throughout that totally dominated any laser scatter or the red emission from the $^4F_{9/2}$ state. In the absence of upconversion, both the laser scatter and the red emission from the $^4F_{9/2}$ state are very strong. This localization of the blue emission near the focus was evidence that the two upconversions, i.e., the blue and the green upconversions, were the result of two separate mechanisms operative at different laser radiation densities. Figure 3 gives the low resolution spectra of the two upconverted emissions together with the red emission from the $^4F_{9/2}$ state. Typical laser-pulse durations were 5–10 ns and pulse energies of about a millijoule were focused to a spot 100 μm in diameter. On the basis of our previous work,[10,11] we assign the blue and the green emissions to $^2G_{9/2}$-$^4I_{15/2}$ and $^4S_{3/2}$-$^4I_{15/2}$ transitions, respectively.

The two-photon dependence of the upconversion was confirmed by studying the dependence of emission intensity on the laser power. Both blue and green emissions followed a quadratic dependence on the pump power, i.e., $I_0 \propto I_{in}^2$ or $\ln(I_0) \propto 2\ln(I_{in})$, where I_0 and I_{in} are the output upconverted emission and the input laser intensities, respectively. This

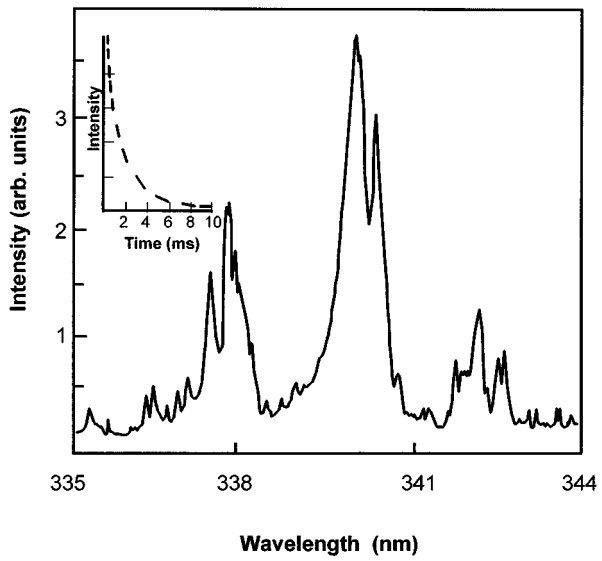

FIG. 4. UV-upconverted signal due to $^2H_{9/2}$-$^4I_{13/2}$ emission as observed by exciting the $^2H_{9/2}$ state by two-photon absorption, $T = 15$ K. The inset shows the time development of the signal following the excitation laser pulse at $\sim 18\,270$ cm^{-1}.

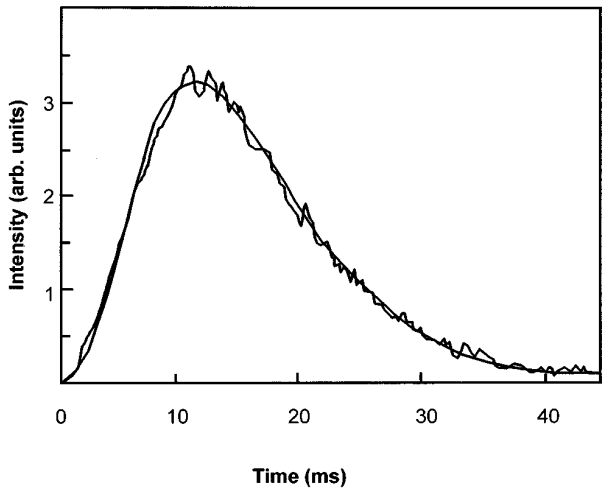

FIG. 5. The time development of the $^2G_{9/2}$-$^4I_{15/2}$ (blue) emission while exciting the $^4F_{9/2}$ with a 10-ns pulse and a pulse frequency of 1 Hz. The solid line gives the theoretical fit assuming the process given by Eq. (7) and solving the rate equations (8).

quadratic dependence is evident in the plot of $\ln(I_0)$ versus $\ln(I_{\text{in}})$ shown in the inset of Fig. 3. It is a straight line with a slope of 2 confirming the quadratic dependence.

Monitoring the excitation spectrum of the blue as well as the green upconversion reproduced the $^4F_{9/2}$ absorption spectrum. However, there was a difference in the relative intensities of the different peaks. They were scaled to the quadratic dependence of the upconversion process, as in Fig. 2.

Radiative lifetimes of the states relevant to upconversion were monitored by directly exciting these states with the pulsed dye laser. These are given in Table III. For some states, particularly the low-lying states, lifetimes are in the tens of milliseconds range. With a high repetition rate of laser pulses there is a considerable probability that a population bottleneck can be formed in these states. This population buildup can lead to the excited-state absorption and subsequently to upconversion. We eliminated this possibility by using a pulse frequency of $\leqslant 1$ Hz. This way the excited ion by the first pulse had sufficient time to radiatively decay to the ground state before the next pulse arrives and therefore no pulse to pulse accumulation of the excitation occurs.

Under cw excitation of the same transition, $^4I_{15/2}$-$^4F_{9/2}$, the blue emission was totally absent and only the green upconversion was observed. In order to distinguish pathways for green upconversion under pulsed and cw excitations the relative intensity of upconverted green and resonant emission from $^4F_{9/2}$ were compared under pulsed and cw excitation conditions. The efficiency of the green upconversion in the cw excitation was much higher than in the pulsed case. This confirmed that the green upconversion under cw excitation is a result of a different upconversion mechanism than that operative under the pulsed excitation.

Another upconversion is observed when $^4S_{3/2}$ is excited in the same manner as $^4F_{9/2}$, i.e., a laser pulse excitation with only moderate pulse energies $\leqslant 1$ mJ. It covers $29\,200$–$29\,700$ cm^{-1} in the UV. The emission is weak and is shown in Fig. 4. It follows a quadratic dependence on the intensity of the exciting radiation suggesting a two-photon process. The time dependence of this UV fluorescence is shown in the inset of Fig. 4. It has a lifetime of <1.2 ms and has no detectable rise time down to 1 ms. Based on the crystal-field calculations presented in Table I, we assign this emission to the $^2H_{9/2}$-$^4I_{13/2}$ transition. Due to very weak signals and subsequent low resolution, a detailed assignment of the spectrum such as that presented for the $^4I_{9/2}$-$^4I_{15/2}$ transition was not possible. However, according to our intensity calculations, the purely electronic transitions are only weakly magnetic-dipole allowed. Almost all of the observed intensity is expected to be in the vibronic transitions involving odd-parity vibrational modes: $v_3 = 255$ cm^{-1}, $v_4 = 110$ cm^{-1}, and $v_6 = 87$ cm^{-1}. Broad features of the spectrum in Fig. 4 are in agreement with this assignment.

Previously reported single-photon absorption spectra of Er in Cs_2NaYCl_6 extend from 6000 to $28\,500$ cm^{-1}. Towards the high-energy side of this range several broad and weak features appear in the single-photon absorption spectrum. They were assigned to the $^2K_{15/2}$ and $^2G_{7/2}$ states.[10,11] Beyond these features no sharp peak was detected. The single-photon absorption at higher energies increases monotonically until the crystal becomes opaque above $30\,000$ cm^{-1}. States lying beyond this limit were not accessible by one-photon absorption. The two-photon absorption has made the $^2H_{9/2}$ accessible and the emission from this state at lower energies were used for the energy assignments of the $^2H_{9/2}$ manifold (*vide infra*).

DISCUSSION

For crystals with high concentrations of optically active ions such as the ones used in the present study, there are many upconversion processes that can occur, especially under intense laser excitation. This greatly complicates any detailed study of upconversion processes. However, some of these processes can be qualitatively differentiated by follow-

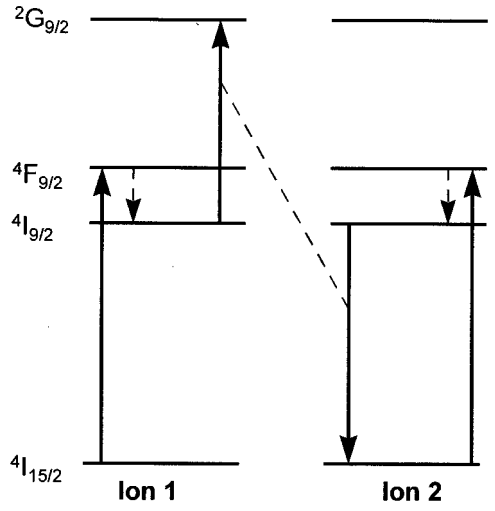

FIG. 6. Schematic representation of the blue upconversion process. Solid bold arrows represent the laser excitation, broken arrows, the nonradiative relaxation, and the dashed line nonradiative multipolar transfer.

ing the time behavior of the upconverted signal and the dependence of the upconversion yield on the concentration of the active ions. Three most relevant upconversion processes for the present case, *step-wise absorption, two-ion energy transfer, and two-photon absorption*, were described earlier. It is possible to isolate these three processes by a careful study of the upconverted signal, that is, its dependencies on the concentration of the active ion, the laser power, and its time evolution.

Blue upconversion

Red to blue upconversion reported in this paper is observable only under intense pulse excitation conditions. It occurs upon excitation in the $^4F_{9/2}$ state. The upconverted signal peaks $\sim$11 ms after the excitation pulse, Fig. 5. This long rise time rules out the TPA to be a possible mechanism for upconversion. Furthermore, there is no state at twice the energy of the exciting radiation as needed for TPA to be operative. By varying the conditions of the experiment, the possibility of step-wise absorption was also eliminated in the following manner. We reduced the frequency of the excitation laser pulses to much less than $1/\tau$, where τ is the lifetime of the longest lived excited state (Table III). With pulse frequencies $\leqslant$1 Hz, we totally eliminated the possibility of any population built up in the excited states and therefore of any step-wise absorption. The blue upconversion was not affected. The blue upconversion also exhibited a strong concentration dependence and was not detected in crystals having less than 1.0 at.% of Er under the experimental conditions described above. Therefore, for the blue upconversion we investigated only the third possibility, i.e., the two-ion energy transfer, in any detail. The blue emission originates from the $^2G_{9/2}$ state. On the conservation of energy grounds, using the energies given in Table I, there are only three possible pathways:

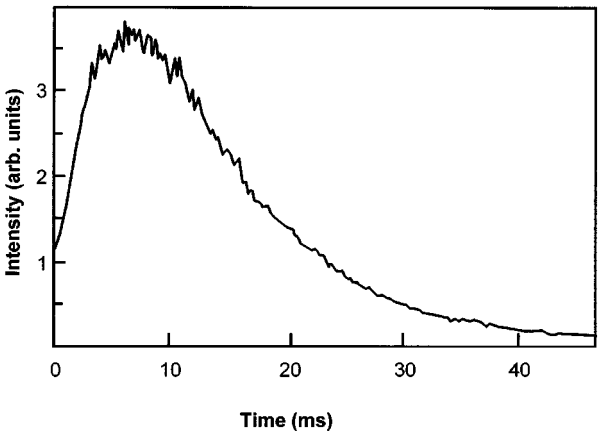

FIG. 7. Time development of the green upconverted signal after exciting the $^4F_{9/2}$ state under the same experimental conditions as for the blue upconversion shown in Fig. 5.

$$(^4F_{9/2})_d+(^4F_{9/2})_a\rightarrow(^4I_{9/2})_d+(^4F_{9/2})_a\rightarrow(^4I_{15/2})_d+(^4G_{9/2})_a \rightarrow(^4I_{15/2})_d+(^2G_{9/2})_a+\text{phonon}, \quad (5)$$

$$(^4F_{9/2})_d+(^4F_{9/2})_a\rightarrow(^4I_{11/2})_d+(^4F_{9/2})_a \rightarrow(^4I_{15/2})_d+(^2G_{9/2})_a, \quad (6)$$

$$(^4F_{9/2})_d+(^4F_{9/2})_a\rightarrow(^4I_{9/2})_d+(^4I_{9/2})_a\rightarrow(^4I_{15/2})_d+(^2G_{9/2})_a, \quad (7)$$

where d and a represent donors and acceptors, respectively.

The time behavior of the upconverted signal is dependent on the lifetimes of all the states involved and therefore it can be used to isolate the above pathways. Rate equation analyses were performed for all the above pathways; only the process represented by Eq. (7), gave a satisfactory fit to the data. In this scheme the process of blue upconversion proceeds like this. Following the excitation of the $^4F_{9/2}$ by the laser pulse, two ions that form the donor-acceptor pair relax to the $^4I_{9/2}$ state. The donor ion then relaxes to the ground state by transfer of excitation to the acceptor that is further excited to the $^2G_{9/2}$ state. Figure 6 gives a schematic diagram of different steps of the process. Rate equations for this process can be written as

$$\frac{dN_1}{dt}=-\frac{1}{\tau_1}N_1,$$

$$\frac{dN_2}{dt}=-\frac{1}{\tau_2}N_2-W(N_2)^2+\alpha N_1,$$

$$\frac{dN_3}{dt}=-\frac{1}{\tau_3}N_3+\frac{1}{2}W(N_2)^2, \quad (8)$$

where τ_1,τ_2,τ_3 and N_1,N_2,N_3 represent the lifetimes and populations of the $^4F_{9/2}$, $^4I_{9/2}$, and $^2G_{9/2}$ states. W is the two-ion transfer rate. α is the rate with which the $^4I_{9/2}$ state is being populated by radiative decay of the $^4F_{9/2}$ states. N_1, N_2, and N_3 are constrained such that the total number of active ions, $N=N_1(t)+N_2(t)+N_3(t)$, and at $t=0$, $N_1(0)=N$, with $N_2(0)=N_3(0)=0$.

A plot of the solution of Eq. (8) is shown by a solid line in Fig. 5. To achieve the best fit, the value of W ranged $980-1200\ s^{-1}$ for various concentrations of Er in different samples. This produced an excellent fit of the time development of the blue upconversion. The other two pathways given by Eqs. (5) and (6) yielded very different time behaviors from the observed one.

A strong two-ion upconversion process is a rather surprising result in our centrosymmetric system where f^n transitions are further restricted by the symmetry of the crystal field. According to Dexter's treatment of the energy transfer[19,20] the probability for the dipole-dipole transfer, P_{dd}, depends on the product of the squares of the transition matrix elements for the donor and the acceptor:

$$P_{dd} \propto (1/r^6)|\langle \Psi_a' | \mu | \Psi_a \rangle|^2 |\langle \Psi_d | \mu | \Psi_d' \rangle|^2, \tag{9}$$

where Ψ_a and Ψ_d are, respectively, the wave functions of the acceptor and the donor separated by a distance r. μ represents the magnetic-dipole operator for purely electronic transitions and electric-dipole operator for vibronic transitions. Matrix elements for both electronic and vibronic transitions in Eq. (9) are generally small for this system;[10] in addition, the minimum distance between lanthanide ions is restricted to 7 Å by the crystal structure, a rather large value. Therefore, we expect P_{dd} to be very small.

For ions at a site of noncubic symmetry, which are generally the subject of energy-transfer studies, a reliable set of wave functions, Ψ's, is difficult to obtain. As a result P_{dd} in expression (9) cannot be calculated theoretically. The usual way taken out of this problem is to use the experimental intensities as observed in emission/absorption spectra in place of the matrix elements in Eq. (9). This has a serious limitation as not all the transitions (real and virtual) involved in the energy transfer are observable in the emission/absorption spectra. Dexter's analysis is therefore only of qualitative use in most cases. However, the present system with the lanthanide ions on a cubic site may be the only exception to this. Here, the number of adjustable crystal-field parameters is a minimum, only two, $\mathbf{B}_0^4$ and $\mathbf{B}_0^6$ in Eq. (3), and a satisfactory set of crystal-field eigenfunctions can be obtained as discussed earlier. Therefore, in principle, it is possible to calculate the energy-transfer probability P_{dd}. However, this is not as simple as may appear at the first glance. In centrosymmetric systems the electric-dipole intensity is distributed throughout the vibronic spectra involving mostly odd-parity localized vibrational modes. The expression for the transfer probability should therefore be summed over the entire vibronic spectrum; in other words, the Ψ's in Eq. (9) should be the vibronic wave functions if μ is the electric dipole operator. For the present case the odd-parity modes of the $(ErCl_6)^{3-}$ molecular unit that contribute most of the intensity in the optical spectrum can be coupled with the electronic wave functions in a Born-Oppenheimer fashion to form the vibronic wave functions. We have earlier reported[10] the electric-dipole intensities and simulated the vibronic spectra using the above procedure. In a similar fashion, it is possible to calculate the transfer probabilities for all vibronic transitions required for Eq. (9). This approach, although good for first-order estimates of vibronic intensities, is of limited use for quantitative comparisons. This is because of two reasons. (1) Higher-order vibronic interactions cause splittings of vibronic lines that may change the energy resonance conditions. (2) The contributions from the lattice modes to the dipolar vibronic intensities are significant as seen in the vibronic spectra. Both of these effects are not incorporated in the simple model described above. Following a similar theoretical approach[21] to calculate the energy-transfer parameters, Moran, May, and Richardson have found that the calculated values from multipole-multipole interaction fall short of observed transfer rates between Tb (donor) and Eu (acceptor) by six to seven orders of magnitude. These authors have suggested a ligand mediated energy transfer that involves virtual excitation of Cl^- ions on the $(R_ECl_6)^{3-}$ molecular unit. If this is the case, efficient energy transfer among rare-earth (R_E) ions should be a common occurrence in this host, i.e., hexachloroelpasolites. The present study gives at least another example of extraordinarily efficient energy transfer needing a satisfactory mechanism to be proposed.

Green upconversion

Knowing that the blue emission results from the population of the $^2G_{9/2}$ state we probed the emission from this state by direct excitation. Under identical experimental conditions as used in the upconversion experiment, the direct excitation of the $^2G_{9/2}$ state produced only the blue emission with no detectable green emission. This conclusively proved that the green upconversion uses a different pathway than the blue and probably a different mechanism is responsible for it.

The green emission originates from the $^4S_{3/2}$. Following the excitation of the $^4F_{9/2}$ state, based on the conservation of energy, there are the following two possibilities for the $^4S_{3/2}$ state population:

$$(^4F_{9/2})_d + (^4F_{9/2})_a \rightarrow (^4I_{9/2})_d + (^4F_{9/2})_a \rightarrow (^4I_{13/2})_d + (^4F_{7/2})_a \rightarrow (^4I_{13/2})_d + (^4S_{3/2})_a + \text{phonons}, \tag{10}$$

$$(^4F_{9/2})_d + (^4F_{9/2})_a \rightarrow (^4I_{9/2})_a + (^4I_{13/2})_d \rightarrow (^4I_{15/2})_d + (^2H_{11/2})_a \rightarrow (^4I_{15/2})_d + (^4S_{3/2})_a + \text{phonons}. \tag{11}$$

Both of these pathways, Eqs. (10) and (11), would explain the observation that the green emission emanated from the entire crystal as opposed to the blue emission that was confined to the focused spot. The blue emission by process (7) requires two ions to be simultaneously in the $^4I_{9/2}$ state and at the same time close enough to enhance the probability of energy transfer under tight focusing conditions. The probability of this happening is highest around the focused region. In contrast, the green upconversion neither by Eqs. (10) nor (11), requires the donor-acceptor pair to be in the same state. Therefore, the green upconversion should be more delocalized in comparison to the blue. For Eq. (10) to be the pathway, the $^4S_{3/2}$ emission should reach a maximum within the lifetime of the $^4F_{9/2}$ state, i.e., ~ 6 ms. The rise time of the green emission should be faster than the blue emission. Both of these effects are observed in Fig. 7, which shows the time development of the green emission after the excitation pulse. This behavior indicates that the pathway (10) is definitely a dominant one for the green upconversion. However,

the theoretical fit using this pathway was not as good as the one obtained for the blue emission. This could partly be due to some contribution from process (11) and partly from the trapping of the emitted red photons, i.e., the radiative transfer. Both of these processes will alter the time development of the signal significantly.

Our identification of the blue upconversion via pathway (7) and the green mainly via pathway (10) also explains the greater efficiency of the green upconversion, as is the observed case (Fig. 3). It should be noted that the efficiency of the green emission relative to the blue emission can only be underestimated from Fig. 3. In contrast to green emission, which emanates from all parts of the crystal, the blue emission is confined to the focused spot facing the detector. A precise comparison of the efficiency of the two upconversions requires relative intensities of the $^4F_{9/2}$, $^4S_{3/2}$, and $^2G_{9/2}$ emissions integrated over the entire energy range as well as the entire solid angle of 4π. Therefore, from Fig. 3 only a rough estimate of the relative efficiency of the upconversion can be made.

The green upconversion is also observed under the cw excitation of the $^4F_{9/2}$ state with an Ar-ion pumped dye laser. The cw power was ~ 10 mW. However, under cw excitation only the $^4S_{3/2}$ state is populated and no blue emission is observed. In this case, step-wise absorption involving long-lived states such as $^4I_{13/2}$, $^4I_{9/2}$, etc., is the dominant mechanism for upconversion. Such upconversions have been reported for a large number of Er-doped systems.[22–25]

UV upconversion

The third upconversion observed was a green to UV upconversion. This was observed pumping in the vicinity of the $^4S_{3/2}$ state. In this case, the $^2H_{9/2}$ ($E > 36\,000$ cm^{-1}) was populated and subsequently the $^2H_{9/2}$-$^4I_{3/2}$ emission centered at 29 500 cm^{-1} was observed, Fig. 4. The excitation pulse energy was $\sim 18\,270$ cm^{-1}. The onset of this upconversion is below the $^4I_{15/2}$-$^4S_{13/2}$ absorption band. This upconversion is seen only with a powerful pulsed laser excitation.

For this particular case, there are at least three possible mechanisms of upconversion. First, the excitation energy lies too close to the $^4S_{3/2}$ state. Therefore, a two-ion transfer such as discussed for the red to blue upconversion is a possibility. Based on the conservation of energy, this process would require both ions to be in the $^4S_{3/2}$ state. The upconversion will be observed when an ion in the $^4S_{3/2}$ transfers all of its energy to another excited ion exciting it to the $^2H_{9/2}$ state. This possibility can be easily ruled out. Had it been that case, the population buildup in the $^2H_{9/2}$ state would be dependent on the lifetime of the $^4S_{3/2}$ state which is ~ 6 ms at 15 K (Table III). The upconverted emission, on the other hand, does not have any detectable rise time and its lifetime is < 2 ms, inset of Fig. 4. The remaining two possibilities are (1) stepwise absorption within a single laser pulse involving the $^4S_{3/2}$ state, and (2) the two-photon absorption in the $^2H_{9/2}$ state. In both of these cases an instantaneous buildup of population in the $^2H_{9/2}$ state will be seen under the time resolution of our experiment ($\sim 1\ \mu$s). In addition, no rise time will be seen for the emission shown in Fig. 4. However, there are at least two major differences between the TPA and the step-wise absorption. First, for the stepwise absorption to occur, the excitation spectrum of the upconverted signal should replicate the one-photon absorption of the $^4S_{3/2}$ state, as we have seen for the blue and green upconversions discussed earlier. Second, stepwise absorption should also be observable under excitation with a cw laser source. In our experiments, no UV upconversion was observed under cw excitation and also the excitation spectrum showed no resemblance to the $^4I_{15/2}$-$^4S_{3/2}$ absorption. This was taken as the proof that the $^2H_{9/2}$ state was populated by two-photon absorption.

TABLE III. Lifetimes of excited states of Er^{3+} in $Cs_2Na_xEr_{1-x}Cl_6$ at 15 K.

State	τ (ms)
$^4I_{9/2}$	11.8±0.3
$^4F_{9/2}$	6.0±0.2
$^4S_{3/2}$	5.9±0.2
$^2G_{9/2}$	3.2±0.1
$^4G_{11/2}$	1.5±0.3
$^2H_{9/2}$	2.0±0.2

For Er^{3+} ion at a site of inversion symmetry, single-photon f^n transitions are only weakly allowed by magnetic-dipole selection rules. However, they become electric-dipole allowed under two photon selection rules. According to our calculations, the $^2H_{9/2}$ state has $\sim 14\%$ mixing of the other spin quartets of the f^n configuration. This relaxes the spin selection rule for the otherwise forbidden $^4I_{15/2}$-$^2H_{9/2}$ transition. Consequently, a weak TPA signal is seen for this transition and only at high radiation densities.

At low temperatures, when only the lowest crystal-field state of $^4I_{15/2}$, i.e., $^a\Gamma_8$, is populated, the excitation spectrum for the UV emission should give $^4I_{15/2}(^a\Gamma_8)$-$^2H_{9/2}$ spectrum. According to the TPA selection rules it should be dominated by purely electronic f^n transitions as well as some vibronic transitions associated with even-parity vibrational modes of the $(ErCl_6)^{3-}$ complex. The UV emission signals were very weak and a detailed excitation spectrum could not be recorded. Furthermore, the presence of strong one-photon $^4I_{15/2}$-$^4S_{3/2}$ absorption in resonance with the exciting radiation complicated the spectra.

As evident from Table I, the calculated and the observed energy levels of the f^{11} configuration differ by ~ 20 cm^{-1}. These differences are the values of Δ given in the last column of Table I. The calculated value of the highest crystal-field component of $^2H_{9/2}$ lies at 36 345 cm^{-1}, about 195 cm^{-1} below the two-photon absorption peak at 36 540 cm^{-1} (twice the excitation energy 18 270 cm^{-1}). We attribute this peak to a vibronic two-photon transition involving an even-parity mode, $^4I_{15/2}$-$^2H_{9/2}(^b\Gamma_8)+\upsilon_{\text{even}}$. This gives the position of the $^2H_{9/2}(^b\Gamma_8)$ to be at 36 345 cm^{-1}.

The $^2H_{9/2}$-$^4I_{13/2}$ emission shown in Fig. 4 is a single-photon spectrum. In contrast to TPA it is dominated by electric-dipole allowed vibronic transitions. The overall span of the emission spectrum is within ± 30 cm^{-1} of the energy range expected from the crystal-field energies (Table I) and the energies of the odd-parity vibrations of the $(ErCl_6)^{3-}$

complex. The position of the lowest crystal-field $^2H_{9/2}(^a\Gamma_8)$ state as determined from this spectrum is 36 133 cm^{-1}. The crystal-field energies of $^a\Gamma_8$ and $^b\Gamma_8$ should be considered correct only within ± 25 cm^{-1}, first, due to the uncertainty in the energies of the odd-parity vibrations, and second, due to the weak and unresolved vibronic spectra on which these assignments are based.

In light of the above results, it appears that efficient energy transfer is typical of this host. Having noted this peculiarity of the system, we would like to point out that elpasolites are ideal candidates for upconversion studies. $Cs_2NaYCl_6:Er^{3+}$ has many advantages: (1) it is stoichiometric, i.e., a complete range of concentrations can be studied up to fully concentrated $Cs_2NaErCl_6$ crystals, (2) in chloroelpasolites, Er^{3+} ions occupy substitutional sites and are well separated from each other (a minimum separation of 7.6 Å is restricted by the structure of the crystal); therefore, pair formation and multiple sites are not possible that could otherwise complicate any detailed studies of upconversion, (3) lattice vibrations in the chloride host are low in energy $\leqslant 100$ cm^{-1}; therefore, multiphonon relaxation processes are not very effective in reducing lifetimes of the electronic states (such long excited-state lifetimes enhance the probability of upconversion), and (4) a good knowledge of crystal-field energy levels and eigenfunctions that are available in this system greatly helps in identifying pathways and understanding mechanisms for different upconversion processes.

CONCLUSIONS

Efficient red to blue and red to green upconversions have been observed for Er in cubic $Cs_2NaYCl_6:Er^{3+}$ and $Cs_2NaErCl_6$ exciting the $^4F_{9/2}$ state in the red region of the spectrum with a pulsed laser. According to our analysis both of these upconversions are caused by two-ion energy-transfer processes. We have used a rate equation analysis to identify different pathways for upconversions. Under high power pulsed excitation, blue emission arise from a single upconversion mechanism and a single pathway is responsible for it. The two-ion mediated energy transfer of the blue upconversion has been verified by studying the concentration dependence. In crystals containing <1.0 at. % of Er such an upconverted signal is not detectable under our experimental conditions. The green upconversion is the result of at least two different pathways. It is independent of Er concentration and can be achieved upon cw excitation. In the last case, it results from a step-wise absorption and has been observed in many other systems. To our knowledge, this is the first report of an upconversion by two-ion energy transfer in a cubic system.

This highly efficient two-ion upconversion is a rather surprising result especially for centrosymmetric systems such as ours. However, our results are supported by another paper on efficient transfer between Eu and Tb ion pairs in the same host.[21] According to these authors well-known models such as Dexter-Forster,[19,20] Inokuti-Hirayama,[26] and Dornauf-Heber[27] energy-transfer models would not account for the observed efficiency of the transfer in elpasolites. Further investigations are necessary to test this general behavior.

Upconversion by TPA in the $^2H_{9/2}$ state has also been reported TPA has allowed access to this high-lying state unobservable in the one-photon absorption emission spectra reported earlier. Two-photon absorption studies will prove extremely useful in cubic systems such as ours, particularly to test the theoretical models for crystal-field calculations.

Finally, emission and absorption spectra of the $^4I_{15/2}$-$^4I_{9/2}$ transition that were not observed in the previous work and were crucial for understanding the energy-transfer processes under investigation have also been reported. A crystal-field calculation for the energies and intensity calculations gives an excellent fit to the observed spectra and supports our assignments of energy-transfer pathways.

ACKNOWLEDGMENTS

We are thankful to Gino Sampietro formerly of the Australian National University for growing the crystals used in the present study and Francis Karwacki for reading the manuscript. This work was partially supported by Grant No. F49620-96-1-0347 from the Air Force Office of Scientific Research.

[1] F. E. Auzel, Proc. IEEE **6**, 758 (1973), and references therein.
[2] E. Downing, L. Hesselink, J. Ralston, and R. Macfarlane, Science **273**, 1185 (1996).
[3] R. Scheps, Prog. Quantum Electron. **20**, 271 (1996).
[4] D. S. Funk, S. B. Stevens, S. S. Wu, J. G. Eden, IEEE J. Quantum Electron. **32**, 638 (1996).
[5] A. J. Silversmith, W. Lenth, and R. M. Macfarlane, Appl. Phys. Lett. **51**, 1977 (1987).
[6] R. M. Macfarlane, F. Tong, A. J. Silversmith, and W. Lenth, Appl. Phys. Lett. **52**, 1300 (1988).
[7] M. P. Hehlen, G. Frei, and H. U. Gudel, Phys. Rev. B **50**, 16 264 (1994).
[8] N. J. Cockroft, G. D. Jones, and D. C. Nguyen, Phys. Rev. B **45**, 5187 (1992).
[9] F. E. Auzel, J. Lumin. **45**, 341 (1990).
[10] Z. Hasan and F. S. Richardson, Mol. Phys. **45**, 1299 (1982).
[11] A. DiPiante, F. S. Richardson, and Z. Hasan, J. Chem. Phys. **82**, 1102 (1985).
[12] J. B. Gruber, J. R. Quagliano, M. F. Reid, F. S. Richardson, M. E. Hills, M. D. Seltzer, S. B. Stevens, C. A. Morison, and T. H. Allik, Phys. Rev. B **48**, 15 561 (1993).
[13] W. T. Carnall, G. L. Goodman, K. Rajnak, and R. S. Rana, J. Chem. Phys. **90**, 3443 (1989).
[14] J. R. Quagliano, N. J. Cockroft, K. E. Gunde, and F. S. Richardson, J. Chem. Phys. **105**, 9812 (1996).
[15] E. G. Ettinger and T. M. Niemczyk, J. Chem. Phys. **68**, 872 (1978).
[16] L. R. Morss, M. Seigal, and N. Edelstein, Inorg. Chem. **9**, 1771 (1970).
[17] Z. Hasan, S. T. Keany, and N. B. Manson, J. Phys. C **19**, 6381 (1986).
[18] Z. Hasan and N. B. Manson, J. Phys. C **21**, 3351 (1988).

[19] D. L. Dexter, J. Chem. Phys. **21**, 836 (1953).
[20] T. Miyakawa and D. L. Dexter, Phys. Rev. B **1**, 70 (1970).
[21] D. M. Moran, P. S. May, and F. S. Richardson, Chem. Phys. **186**, 77 (1994).
[22] Z. Mazurak, E. Lukowiak, and B. J. Trzebiatowska, J. Lumin. **29**, 47 (1984).
[23] J. P. van der Ziel, F. W. Ostermayer, Jr., and I. G. Van Uitert, Phys. Rev. B **2**, 4432 (1971).
[24] E. Okamoto, M. Sekita, and H. Masui, Phys. Rev. B **11**, 5103 (1975).
[25] N. J. Cockroft, G. D. Jones, and R. W. G. Syme, J. Lumin. **43**, 275 (1989).
[26] M. Inokuti and F. Hirayama, J. Chem. Phys. **43**, 1978 (1965).
[27] H. Dornouf and J. Heber, J. Lumin. **22**, 1 (1980).